Advances in Colloid and Interface Science
94 (2001) 53–81

ADVANCES IN COLLOID AND INTERFACE SCIENCE

www.elsevier.com/locate/cis

Block copolymer thin films: pattern formation and phase behavior

Peter F. Green[a,b,*], Ratchana Limary[b]

[a] *Department of Chemical Engineering and Texas Materials Institute, The University of Texas at Austin, Speedway and 26th Street, Austin, TX 78712-1062, USA*
[b] *Texas Materials Institute, The University of Texas at Austin, Austin, TX 78712, USA*

Abstract

During the last decade, research on thin, sub-micron thick, block copolymer films was devoted toward understanding and controlling microstructural and topographical features at temperatures $T < T_{ODT}$, where T_{ODT} is the order–disorder transition temperature below which thermodynamic interactions favor the formation of ordered (phase separated) microstructures. Symmetric diblock copolymers, the subject of this review, undergo an isotropic to lamellar transition when $T < T_{ODT}$. Topographical features, 'islands' or 'holes,' of these films typically reflect the underlying phase separation; and the dimension of these features, normal to the substrate, is equal to the interlamellar spacing, L. Two aspects of block copolymer thin films that have not received much attention are discussed in this paper: (1) pattern formation in symmetric block copolymers under conditions of $T > T_{ODT}$; and (2) phase behavior of thin film symmetric diblock copolymer/homopolymer mixtures, when $T < T_{ODT}$.

Keywords: Block copolymers thin films; Pattern formation; Phase behavior

Contents

* Corresponding author.
E-mail address: green@che.utexas.edu (P.F. Green).

0001-8686/01/$ - see front matter
PII: S0001-8686(01)00055-0

1. Introduction

Apart from conventional applications such as membranes, lithography and coatings, polymer thin films are of current interest for device technologies such as light-emitting diodes, photodiodes and thin film transistors in which the polymer serves the role of the active material component [1,2]. Films with thicknesses in the sub-micron thickness range are of particular interest in the latter applications. Properties of sub-micron thick films typically differ appreciably from bulk properties due largely to a combination of polymer segment/interfacial interactions and entropy. There is a range of unresolved issues, with varying complexity, depending on whether the material is a homopolymer, an A/B homopolymer blend or a block copolymer thin film.

Changes in properties such as the glass transition temperature, the viscosity and translational chain diffusion coefficients with decreasing film thickness are well documented in these systems. Experiments on homopolymer thin films, for example, indicate that the glass transition temperature may increase, or decrease, with decreasing film thickness [3–9]. Moreover, increases in the viscosity and decreases in translational chain diffusion coefficients of chains near substrates have been shown to occur as well [10–17]. In some regard, the decrease in chain dynamics in the vicinity of the polymer/substrate interface appear to be at odds with reported decreases of the glass transition temperature with film thickness in some systems. The nature of these changes in the translational chain dynamics and in the glass transition with film thickness, and their relation to chain packing effects, excluded volume and entanglement effects near surfaces, together with substrate/polymer interactions, are of current interest to researchers.

In bulk A/B homopolymer mixtures, the phase behavior is determined by a combination of the translational entropy of the chains and the enthalpic interactions between the constituents of the blend. In thin films, entropic effects associated with chain packing and confinement, together with enthalpic polymer segment/segment and segment/interface interactions, affect the phase separation

temperature and the symmetry of the phase diagram [18]. Changes in critical temperature with film thickness, surface directed spinodal decomposition due to a preferential attraction of one component to an interface, and a broadening of the intrinsic interfacial profiles in partially miscible blends due to capillary waves, are well documented in thin film blends [18–49].

Thin film diblock copolymers, to which this paper is devoted, have been the subject of much research during the last decade [50–71]. At temperatures below an order–disorder transition temperature, T_{ODT}, A–b–B diblock copolymers are known to exhibit different microphase-separated morphologies, including: spheres; hexagonally packed cylinders; lamellae; and bicontinuous 'gyroid' structures, depending on the relative volume fractions of the components [72,73]. Symmetric diblock copolymers, for example, undergo an isotropic-to-lamellar transition below the order–disorder transition temperature, when $\chi N > 10.495$. In thin film geometries, the interfacial interactions impose restrictions on the local A/B segmental concentration profiles. The component with the lower surface energy typically resides at the free surface. If the other component resides at the substrate then the lamellae generally orient normal to the substrate. The topography of these ordered films is determined by the commensurability between the local film thickness and the interlamellar spacing. Specifically, the surface of the film is smooth if a different component of the diblock resides at each interface and the local film thickness is $h = H_n = (n + 1/2)L$, where n is an integer. If the same component of the diblock were to reside at both interfaces, the surface is smooth when $h = H_n = nL$. When the thickness of the symmetric diblock copolymer film deviates from the appropriate criteria, $h = H_n$, by an amount $\Delta h > 0$ ($h = H_n + \Delta h$), topographical features, islands, holes and 'bicontinuous' patterns, each of height L, appear at the surface of the film. Examples of these topographies are shown in Fig. 1a–c. The system minimizes its free energy by creating a discontinuous layer instead of forming a complete layer of sub-optimal thickness less than L.

Most of the research on block copolymer thin films has been devoted to examining ordering near surfaces and to controlling the orientation and morphology of samples in the temperature regime $T < T_{ODT}$ using external fields, and by modifying the interfacial interactions [51–66]. This paper addresses two aspects of thin film block copolymer systems that have not received much attention:

1. We first discuss the phase behavior and stability of thin diblock copolymer films above the bulk order–disorder transition temperature.
2. The second topic concerns thin film mixtures of homopolymers and diblock copolymers.

Considerable effort has gone into understanding how homopolymers affect the domain dimensions and phase behavior of bulk diblock copolymer/homopolymer systems while little is understood about these systems in thin film geometries. In particular, we discuss the effects of confinement, polymer/substrate interactions and enthalpic segment/segment interactions on the phase behavior of mixtures of thin film of A–b–B symmetric diblock copolymers with A, B and C homopolymers.

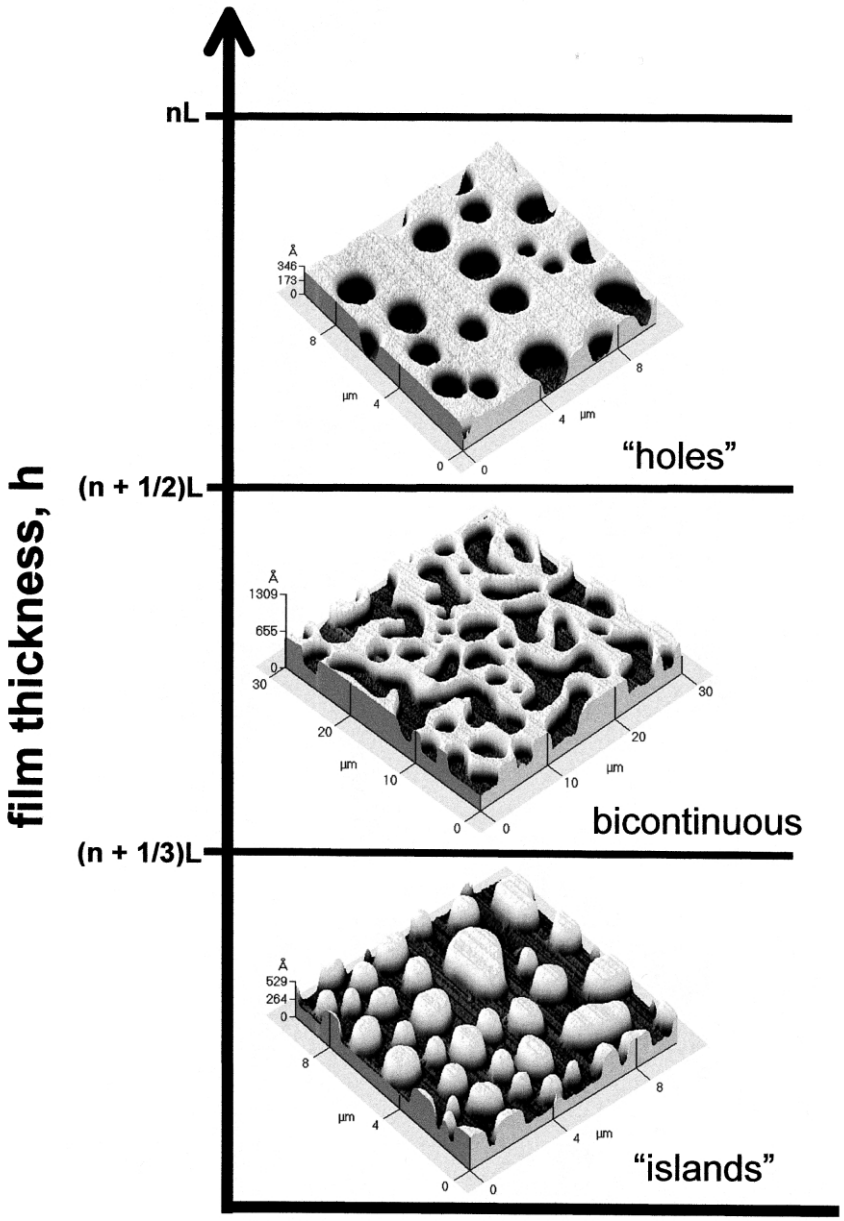

Fig. 1. AFM images of topographical features that appear in ordered ($T < T_{ODT}$), symmetric, PS–b–PMMA diblock copolymer thin films on SiO_x are shown here: (a) islands; (b) bicontinuous; and (c) holes. The height of each topographical feature is equal to the interlamellar spacing, L. In this figure n is an integer.

2. Symmetric diblock copolymers above the order–disorder transition

We show that while copolymers above the ODT exhibit features akin to the behavior of simple homopolymer liquids, they maintain some features that are inherently associated with ordered block copolymer films. Specifically, when the film thickness, h, is thinner than a characteristic thickness, h_L, the film becomes unstable with the spontaneous formation of holes that appear spontaneously at random locations throughout the surface of the film, or by the formation of a 'bicontinuous', "spinodal-like" pattern. Thin homopolymer films exhibit similar behavior [74–80]. The particular pattern is dictated by the initial film thickness, h. When $h = h_L$, the film is stable and the surface remains smooth. However, for films of $h > h_L$, a layer of thickness $h-h_L$, becomes unstable and dewets an underlying layer of thickness h_L, forming a pattern that consists of either holes or a bicontinuous ('spinodal-like') structure. These patterns eventually evolve into droplets on the layer. It appears that the thickness h_L is one-half of the interlamellar spacing, L, of the copolymer in the ordered state.

2.1. Hierarchical pattern formation

We now discuss pattern formation in a symmetric polystyrene and poly(methylmethacrylate) (PS–b–PMMA) diblock copolymer with a total degree of polymerization $N = 200$ and $\chi N = 7.5$. The condition for the isotropic to lamellar transition in a symmetric diblock copolymer is $\chi N > 10.5$, indicating that for this copolymer, $T > T_{ODT}$. We note that the glass transition temperature of the PS component is 100°C and that of PMMA is 115°C. Therefore the T_g of each of these polymers is greater than T_{ODT}.

Films that range in thickness from 2 to 100 nm were prepared on silicon substrates using a photo resist spinner. Toluene was the solvent. The substrate had a native oxide layer of thickness of 2 nm, as determined by spectroscopic ellipsometry. The surfaces of the as-spun copolymer films were smooth. These samples were subsequently annealed at 170°C under vacuum conditions for varying periods of time. Topographical analysis of our samples was performed using an Autoprobe CP (ThermoMicroscopes) atomic force microscope (AFM) after periodically quenching to room temperature. AFM scans were performed in contact, intermittent contact and non-contact modes. In the contact mode experiments, we constrained the stress between the microscope tip and the sample, such that measurements yielded the same results obtained from non-contact and intermittent contact experiments. Our experiments were typically conducted in the contact mode for convenience. Images were processed to remove the curvature due to the bending motions of the scanner during rastering, using the software provided by the manufacturer. The feature sizes were based on averages of numerous line profile measurements of the images.

The experiments reveal that the copolymer exhibits a hierarchy of patterns, depending on the film thickness, as shown in Fig. 2. The results in the figure show that initially smooth films of $h < 35$ nm will spontaneously rupture, creating a

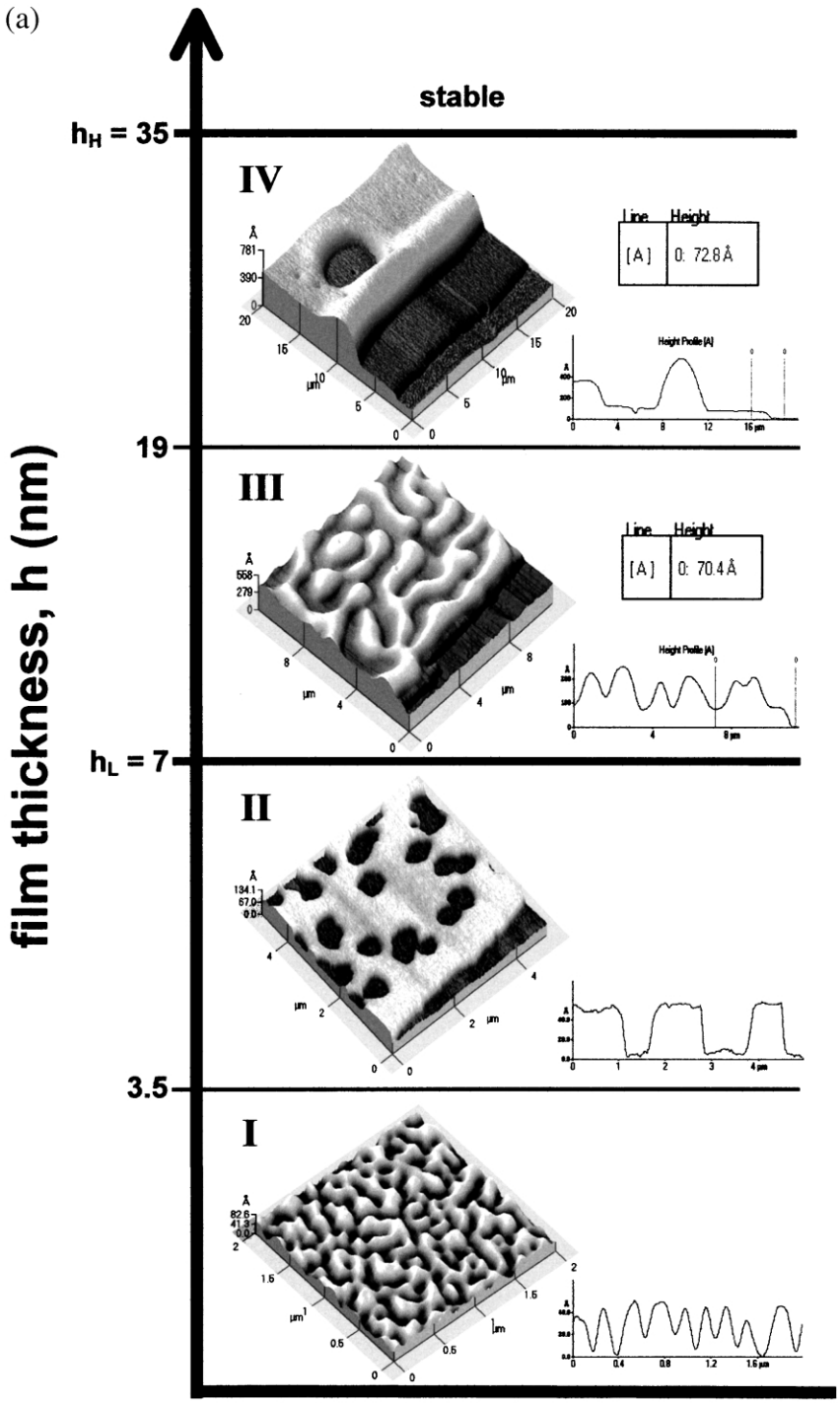
(a)
stable
h_H = 35
19
h_L = 7
3.5
film thickness, h (nm)
IV
III
II
I
Line Height
[A] 0: 72.8 Å
Line Height
[A] 0: 70.4 Å
Height Profile [A]

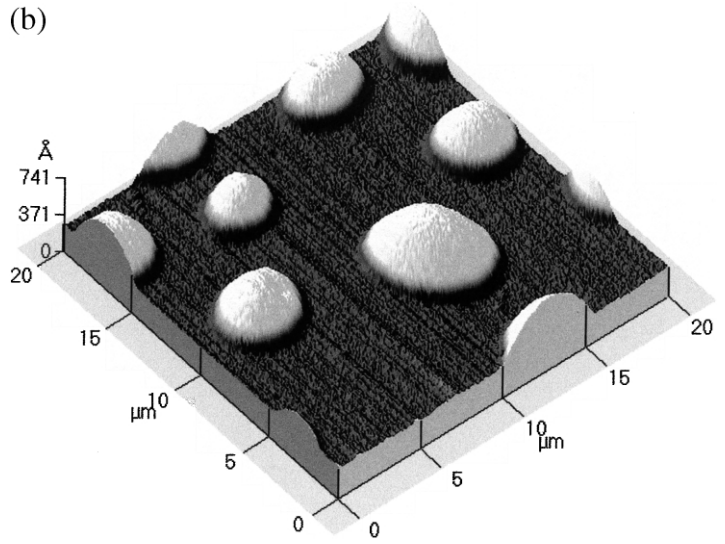

Fig. 2. (*Continued*).

'bicontinuous' structure. The image of the sample shown in section I of the figure was initially $h = 3$ nm and it was annealed for 46 min at 170°C. In contrast, discrete holes appeared in slightly thicker films in the range 4 nm $< h < h_L = 7$ nm (section II). The sequence of patterns is repeated for films of $h > h_L$. In the thickness range 7 nm $< h <$ 19 nm, a 'bicontinuous' topography is observed (section III), whereas discrete cylindrical holes appear randomly throughout the surface of films in the thickness range 19 nm $< h <$ 35 nm. Section IV shows a hole near the edge of the film (see also Fig. 4b). Films thicker than 35 nm are stable with smooth surfaces.

The instabilities in these films can be understood in terms of the effect of long and short-range intermolecular forces on thin films [74–100]. The condition for partial or complete wetting of a small liquid droplet is dictated by the spreading coefficient, $S = \gamma_{sv}(\gamma_{lv} + \gamma_{sl})$, where γ_{sv} is the interfacial energy between the solid and the vapor phase, γ_{lv} is the liquid/vapor interfacial tension and γ_{ls} is liquid/solid interfacial tension. $S < 0$ and $S > 0$ correspond to partial and complete wetting, respectively. For a large droplet, the equilibrium thickness, h_{eq}, is

Fig. 2. Topographical features spontaneously appear in thin PS–b–PMMA diblock copolymer films, $T > T_{ODT}$. (a) The images in this figure show that the pattern depends on the film thickness. For $h < 3.5$ nm, a 'bicontinuous' structure evolves, whereas holes appear randomly throughout the surface of the film for $3.5 < h < 7$ nm. When 7 nm $< h <$ 19 nm, an 'autophobic' dewetting process occurs whereby a layer of the sample of thickness $h_d = h - 7$ nm, becomes unstable and forms a bicontinuous structure on an underlying layer of thickness $h_L = 7$ nm. When 19 nm $< h <$ 35 nm, holes appear randomly throughout the surface of the film. (b) The final state of the film is characterized by droplets of copolymer on the underlying substrate.

influenced by gravitational forces and is $h_{eq} = (2S/\gamma_{lv})\kappa^{-1}$, where κ is the capillary length. Brochard and coworkers pointed out that thin films of thickness $h > h_{eq}$ should remain stable [77].

Polymer films with thicknesses $h < h_{eq}$, and typically 100 nm or thinner, are subject to destabilizing long-range intermolecular forces and may spontaneously rupture, creating patterns that reflect variations in the local film thickness. The topographies are bicontinuous patterns [74,76–79], discrete *cylindrical holes* [74,75,77,79], and highly asymmetric holes [80] that appear throughout the surface of the film. The structural evolution of each of these patterns is distinct. The origin of pattern formation is associated with the fact that small amplitude modulations at the surface of a thin liquid film can become amplified by the long-range van der Waals intermolecular forces. Brochard described the surface undulations in a thin film on a substrate using linear stability analysis [77]:

$$h(x,t) = h_d + \delta h \exp(t/\tau) \tag{1}$$

In this equation h_d is the initial film thickness and

$$\delta h = \delta h_d \exp(iqx) \tag{2}$$

is the amplitude of the fluctuations. The dominant wave vector describing the fluctuations was predicted to be:

$$q_m = \left(\frac{A}{4\pi\gamma}\right)^{1/2} \frac{1}{h_d^2} \tag{3}$$

where A is the Hamaker constant and γ is the interfacial energy. The dominant relaxation time associated with the growth of the fluctuations is:

$$\tau_m^{-1} = \frac{A^2}{48\pi^2} \frac{1}{\gamma\eta h_d^5} \tag{4}$$

This theory predicts that for dewetting to occur, the van der Waals forces should be attractive ($A > 0$). The Laplace pressure, the ratio of the surface tension to the local film thickness, acts to stabilize the film. The disjoining pressure, which accounts for the tendency of the film to adjust its thickness to minimize the free energy, together with the Laplace pressure, determine the critical wave length beyond which the instability will grow. Fluctuations can grow to the height of the initial film thickness whereby rupturing occurs. The relaxation time of the instability is determined by the Laplace pressure, the disjoining pressure and by the viscosity.

The short-range forces, together with the long-range forces, determine the morphology of the disrupted film [79]. Recently, Sharma and Khanna performed a series of simulations that accounted for effects due to short-range polar forces and

long-range forces [75,79]. They suggested the following expression for the excess free energy:

$$\Delta G = \frac{-A}{12\pi h_{\mathrm{d}}^2} + S^{\mathrm{P}} e^{-h_{\mathrm{d}}/l} \tag{5}$$

where the first term describes the long-range forces and the second, the short-range forces. In this equation S^{P} is the polar component of the spreading coefficient and l is a short-range cutoff length. Their results suggest that the morphology is determined by a combination of short and long-range forces.

2.2. Evolution of the 'bicontinuous' structure

The time-dependent structural evolution of the 'bicontinuous' ('spinodal-like') pattern of films in the thickness range 7 nm $< h <$ 19 nm is now discussed. An 'autophobic' dewetting process occurs, whereby a layer of material of thickness $h_{\mathrm{d}} = h - h_{\mathrm{L}}$ dewets an underlying layer of thickness $h_{\mathrm{L}} = 7$ nm, anchored to the substrate. That the thickness of the underlying layer is 7 nm is evident from the line profile of the edge of the film in sections III and IV of Fig. 2. It appears that the thickness $h_{\mathrm{L}} = 7$ nm corresponds to one-half of the interlamellar spacing of the diblock copolymer if the copolymer were in an ordered state (this is addressed in more detail in Section 3.2). The final state of the film is characterized by droplets on the layer of height $h_{\mathrm{L}} = 7$ nm.

Fast Fourier transforms of AFM images of this pattern were taken during different stages of evolution. The dominant wave vector of the fluctuations, q_{d}, was extracted from each image. The decrease in the q_{d} with time can roughly be approximated as $t^{-1/3}$ during the interval 20–72 min, as shown in Fig. 3a. Linear stability analysis, Eq. (3), indicates that the wave vector should remain constant, whereas our data show that it decreases with time. This may be a result of the fact that the linear regime, where the wave vector is constant, occurs at times earlier than were examined with the AFM. Nevertheless, one should expect q_{d} to decrease with time as the fluctuations grow. Simulations by Milchev and Binder indicate that the wave vector should decrease as $t^{-0.38}$, which is comparable to our data [81]. We should caution, however, that preliminary results in our laboratory indicate that the growth of the fluctuation might be sensitive to the short-range interactions with the substrate. If this indeed turns out to be the case, then the time-dependence of q_{d} in this regime is not universal. This could be the reason that q exhibited weaker time-dependence in the polystyrene/Si system as reported by Xie et al. [78]. A final resolution to these issues will await further experiments and theory.

It is worthwhile to examine how the thickness fluctuations, δh, increase during the same interval, $t < 72$ min. The thickness fluctuations were extracted from averages of numerous line profile measurements of the samples. It is clear from Fig. 3b that the increase in $\delta h/h_{\mathrm{d}}$ with time is consistent with an exponential

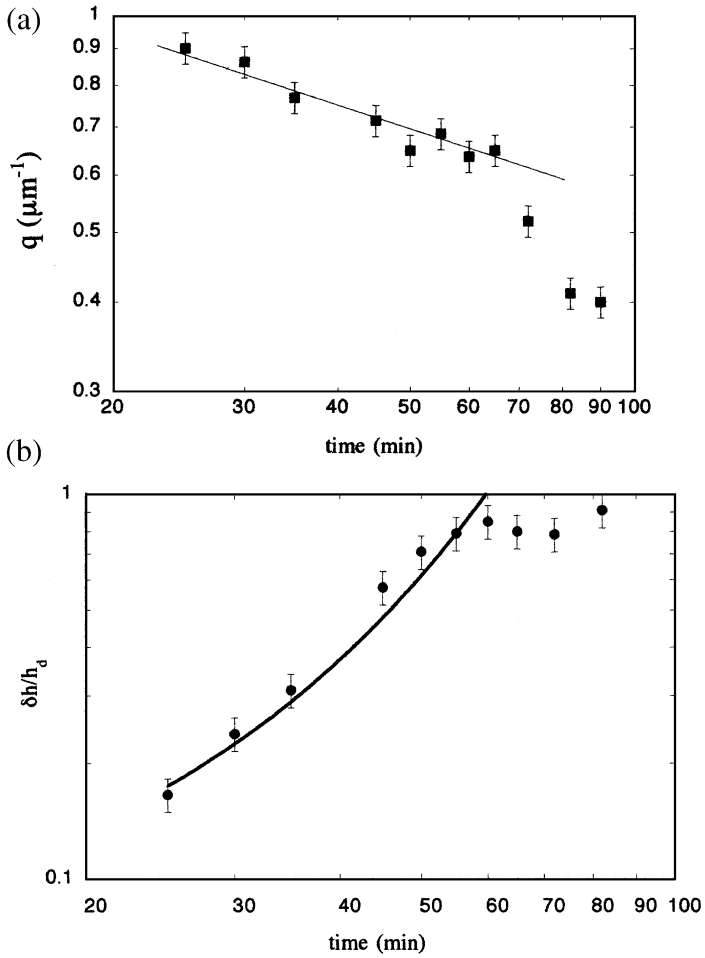

Fig. 3. (a) The time dependence of the dominant wave length fluctuations is plotted here. (b) The dependence of the thickness fluctuations, $\delta h/h_d$, is shown here.

dependence, as suggested by Eq. (2). This relaxation time, which depends on A, h_d and γ, was determined to be 20 s from a fit to the data. The underlying substrate is exposed when $\delta h/h_d > 1$, and this occurs after approximately 72 min. Below we discuss the structural evolution of the pattern shown in Image 4 of Fig. 2.

2.3. Dynamics of holes

We now direct our attention to the morphology that evolved as a result of the nucleation and growth of holes for films of $h > 19$ nm (section IV). Dewetting proceeded with the formation of discrete holes without their characteristic peripheral rims (Fig. 4a). During this early stage, the hole radius, R, increased exponen-

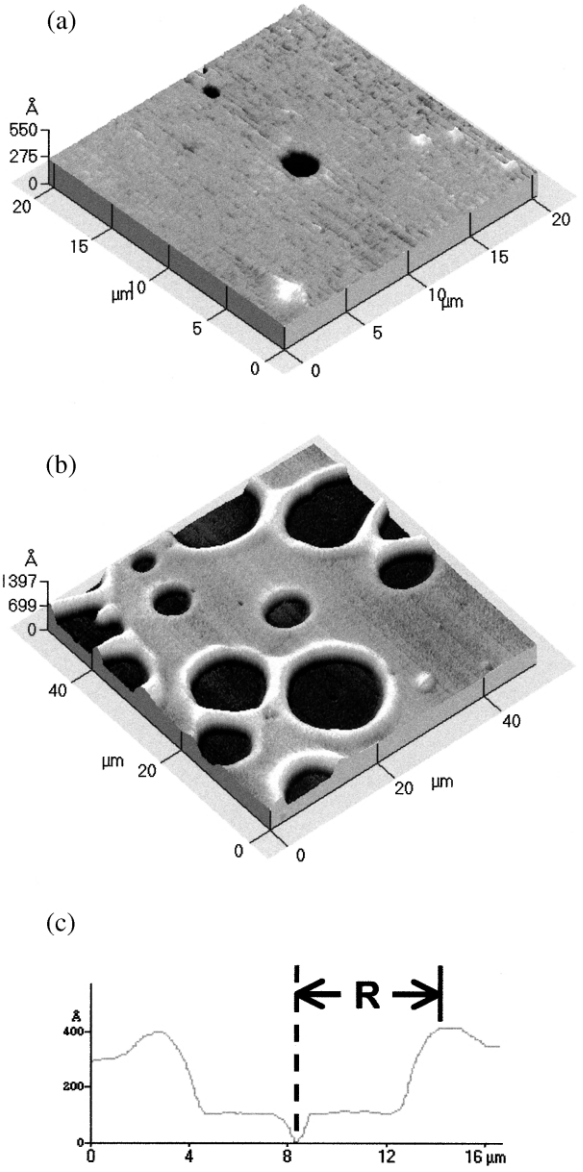

Fig. 4. (a) The early stage development of a hole, before the development of the characteristic rim is shown here. (b) Fully developed holes with its characteristic rims are shown here. (c) A typical line scan of a hole is shown here. R is the radius of the hole.

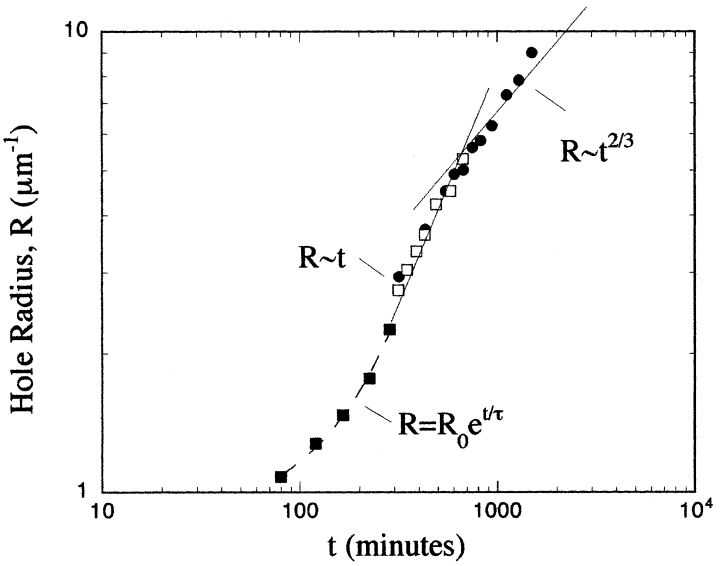

Fig. 5. The three stages of hole development are reflected in the dependence of the growth of the radius, R, as a function of time. At early times, the growth is consistent with an exponential dependence. During intermediate times, the growth is consistent with a linear time dependence, whereas $R \sim t^{2/3}$ at later times. The holes later impinge to form an interconnected structure, which decays to form droplets.

tially with time. This stage was followed by a narrow intermediate regime where the rim develops (Fig. 4b) and $R \sim t$. Fig. 4c shows a line scan of an actual hole from which R is determined. When the rim was fully developed, $R \sim t^{2/3}$. At the final stage of the process, droplets of the copolymer, a few microns in diameter and heights on the order of tens of nanometers, existed on a dense copolymer 'brush' of uniform thickness 7 nm anchored to the substrate. Fig. 5 summarizes the dependence of the hole radius, R, as a function of time during the three stages. These data were determined from two isolated holes. The margin of error in measurement is approximately the size of a point on the graph.

Brochard and coworkers predicted three stages of hole growth during dewetting of a thin homopolymer film [87]. If the deformation in the film is assumed to be elastic and the viscous dissipation at the film/substrate interface is negligible, then, when the underlying substrate is exposed, the radius of the hole should increase as:

$$R(t) = R_0 e^{t/\tau} \tag{6}$$

Our data indicate that the exponential dependence occurs much earlier during the process. Using Eq. (6), the relaxation time, τ, determined from the data in Fig. 5 is 200 min. It is difficult to make a comparison between τ and the translational tracer

diffusion of this diblock chain, since τ is a function of the film thickness, h, S and the viscosity, η.

At longer times the film behaves like a viscoelastic liquid, where the chains can undergo translational motions. The rim is created when the radius, R, of the hole reaches a critical value $R_C = (bh)^{1/2}$, where b is the hydrodynamic extrapolation length, the length over which velocity profile extrapolates to zero. At the melt/substrate interface, b characterizes slip. It is inversely proportional to the coefficient of friction, k, between the melt and the substrate, $b = h/k$.

During the second stage, $R > R_C$ and viscous dissipation at the melt/substrate interface provides the dominant contribution. The velocity is constant for this intermediate regime, during which the rim becomes fully developed and

$$R = (S/\eta)(b/h)^{1/2}t \tag{7}$$

Here the viscous forces balance the capillary driving forces. In an earlier publication we showed that the rim does indeed develop in the regime that denotes the transition of the linear dependence of R on t from its exponential dependence [96].

Finally, the late stage growth of the hole, with its completely developed rim, exhibits a power law dependence:

$$R = t^{2/3} \tag{8}$$

This prediction is based on the assumption that the viscous dissipation is dominated by the dissipation in the liquid substrate. The decrease in the growth rate results from the fact that while the driving force for spreading and dewetting remains constant, the resisting friction force increases with the size of the rim. Hamley and coworkers observed a $t^{2/3}$ dependence in the late stage autophobic dewetting of a diblock copolymer film [90].

We just showed that for $T > T_{ODT}$, thin diblock copolymer films exhibit a hierarchy of morphologies that depend on the thickness of the film. While these morphologies have been observed in homopolymer films, there are distinct differences. For example, the hierarchical formation, islands, 'bicontinuous' and holes, is unique to copolymers. Moreover, the formation of the anchored layer of thickness $h_L = 7$ nm, is not observed in homopolymers. In fact, we believe that h_L is one-half the interlamellar period of this copolymer if it were ordered, as discussed later. There are two outstanding questions that are yet to be addressed. The first is the analysis of the complete structural evolution of the bicontinuous pattern toward the formation of droplets. The dynamics could be compared to the coarsening of islands examined by Bassereau et al., in PS–b–PMMA diblocks in the ordered state, $T < T_{ODT}$ [52]. Secondly, it would be worthwhile to compare these dynamics to the dynamics of spinodal decomposition of binary mixtures. In spinodal decomposition, the order parameter describes composition fluctuations, whereas in dewetting, the order parameter describes thickness fluctuations. The formation of the layer of thickness, h_L, is of particular interest since it strongly suggests the existence of a substrate-induced ordering of the copolymer above the bulk ODT of

the material. In this regard, further experiments and theory should provide insight into the surface-induced ordering in these systems.

In the section that follows, we briefly discuss the behavior of thin diblock copolymer films under conditions of $T < T_{ODT}$, where thermodynamics favor ordered, microphase-separated, structures.

3. Block copolymers mixtures below the ODT

Mixtures of dissimilar polymers are often produced in order to achieve properties that are superior to the individual constituents. However, in situations in which the constituents are incompatible, the mechanical properties of these compositionally heterogeneous mixtures are poorer than those of their constituents. The interfacial tension between the domains is large, so it is difficult to create materials in which one phase can be finely dispersed in the other. Moreover, the interfacial adhesion in these systems is weak. The addition of block copolymers to the mixture tends to alleviate the problem. During the past two decades, research on block copolymer/homopolymers has concentrated in two general directions. In the first, questions evolve around the interfacial activity of the copolymers in the mixture. In the second, the block copolymer forms the major phase and the effect of the addition of homopolymers to the structure and to the properties of the copolymer is examined. The remainder of this paper is devoted to the latter.

The manner in which homopolymers affect the structure of block copolymers is reasonably well understood [101–115]. When homopolymer chains, A and B of degree of polymerization, N, are added to an A–b–B diblock copolymer of degree of polymerization N_C, where $N_C > N$, the homopolymers segregate to the appropriate copolymer domains in order to minimize the number of unfavorable segment/segment contacts to decrease the overall free energy. Consequently, the domains swell in order to accommodate the homopolymer chains. The degree of swelling is determined by φ, the volume fraction of the homopolymer chains, N and N_C, as discussed in detail later. In addition to domain swelling, the addition of homopolymer chains can induce a change of the microstructure of the copolymer, order–order or order–disorder transitions. When the homopolymer chains are much longer than the copolymer chains, they segregate to form a separate phase. While much is known about bulk systems, we understand little about the influence of film thickness constraints and of polymer/substrate and polymer/free surface interactions on miscibility in thin films of diblock copolymer/homopolymer systems.

The remainder of this paper is devoted to misciblity in thin film mixtures of homopolymers with symmetric diblock copolymers. We show that order–order transitions can be frustrated in thin film mixtures. Moreover, the dependence of the microphase-separated, or ordered, domain thickness, L, on the homopolymer volume fraction is a function of the proximity of the layer from the substrate. Furthermore, we show how the substrate can influence copolymer/homopolymer miscibility in thin films. We begin with a brief discussion of the phase behavior and

formation of the topography of pure diblock copolymers in the ordered state, below the ODT, in order to provide a context for the subsequent discussions.

3.1. Symmetric diblock coplymers below the ODT

When the temperature is decreased below T_{ODT}, the A–b–B diblock copolymer decreases its free energy by reducing the number of unfavorable A/B, enthalpic, contacts. This is accompanied by a reduction in translational entropy of the chains. The A-rich and B-rich domains grow in order to increase the surface to volume ratio. In an effort to maintain a constant segmental density throughout this process, the copolymer chains must stretch beyond their equilibrium conformations. In the strong segregation regime ($\chi N \gg 10.5$) one can show that for symmetric diblock copolymers, the equilibrium interlamellar spacing, L_0, can be obtained from a balance between the elastic stretching energy and the interfacial energy contributions [73]:

$$L_0 \propto \chi^{1/6} N^{2/3} \tag{9}$$

Atomic force microscopy provides a simple way to measure L in thin diblock copolymer films on substrates. Consider the situation of a thin PS–b–PMMA diblock copolymer film on an SiO_x substrate. One of the diblock components has a strong preferential affinity for the substrate and the other for the free surface.

Specifically, we examined the properties of a symmetric PS–b–PMMA diblock copolymer of degree of polymerization $N = 640$ ($N_{PS} \approx 317$, $N_{PMMA} \approx 325$) and of $\chi N \gg 10.5$ ($T < T_{ODT}$). Films were prepared on silicon substrates from toluene/copolymer solutions using a photoresist spinner. The substrate had a native SiO_x layer that was 2 nm thick, as measured using ellipsometry. The films were subsequently scored and annealed under vacuum conditions at 170°C for varying periods of time, from 8 to 190 h. The films were then analyzed using atomic force microscopy, as described earlier.

A film with a thickness that varied in height throughout the sample. The topographical features at different regions of this film are determined by the local film thickness, h_{local}. The film was scratched to expose the substrate after annealing. A point was then arbitrarily identified at the edge of the film as the origin. AFM scans were performed at the edge of the film in the direction of increasing film thickness. h_{local} was determined along with the AFM scans. A series of terraces of quantized heights $H_n = (n + 1/2)L$ developed during the annealing process to accommodate the increase in h_{local} when h_{local} increased in height beyond L from its value at the origin. The information presented in Fig. 6 summarizes the results for a PS–b–PMMA film. In this film, h_{local} increased from $h_{local} = H_4 + \delta h$, where $H_4 = (4 + 1/2)L$, to $h_{local} = H_6 + \delta h$, [$H_6 = (6 + 1/2)L$], a lateral distance of 1500 μm away. At the origin, the height of the first terrace is H_4, and the topography of this region consists of islands of height L (see Fig. 1a). This region is identified with the letter 'I', in Fig. 6. As h_{local} increased, the density of islands increased until they formed an interconnected structure (Fig.

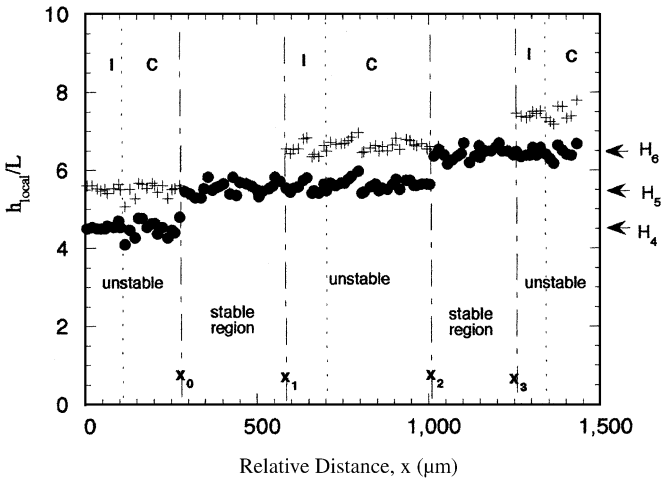

Fig. 6. This figure shows how the topography of a thin film that increases in thickness from approximately $h_{local} = 4.6\ L$, at the origin, to 7.2 L at 1500 μm away. The sample surface rearranges, locally, into terraces of height $h = H_n$. The topography on each terrace consists of islands (identified by 'I') or interconnected (bicontinuous or holes) structures (identified by 'C') to accommodate the excess layer of material of thickness less than L. The regions identified as 'stable' are flat regions on which there are no topographical features since $h_{local} = H_n = (n + 1/2)L$. The filled circles in this figure indicate the local height of the terraces and the plus signs (+) represent the local height of the structures above the substrate.

1b). This region of the figure is identified with the letter 'C.' When h_{local} increases further, holes are formed, Fig. 1c, and as more material becomes available (increasing local thickness), the next terrace of height, $h_{local} = H_5$, forms. Islands appear on this new terrace of height H_5, as more material becomes available. The process is repeated on this terrace, until a new terrace of height, H_6, forms. In general, we determined that islands are formed when $\delta h < L/3$, a bicontinuous structure is formed when $L/3 < \delta h < L/2$, and holes are formed when $L/2 < \delta h < L$. The system minimizes its free energy by forming a discontinuous layer of thickness L, rather than forming a complete layer of sub-optimal thickness less than L. Clearly, the topographies form to accommodate the excess material not used to create a complete layer.

An additional topographical feature exists in these systems. Steps appear at the edge of films that are scored prior to annealing. An example of these steps is shown in Fig. 7. The first step, in contact with the substrate, is of height $L/2$ and all others are of height L. The steps are indicative of a microphase-separated, quantized structure and have been reported in other ordered copolymer systems. However, the existence of the steps and the surface topographical features are characteristic of lamellar systems.

The topographies discussed above are a result of the interactions of the microphase-separated diblock copolymer with the substrate. If the sample is suffi-

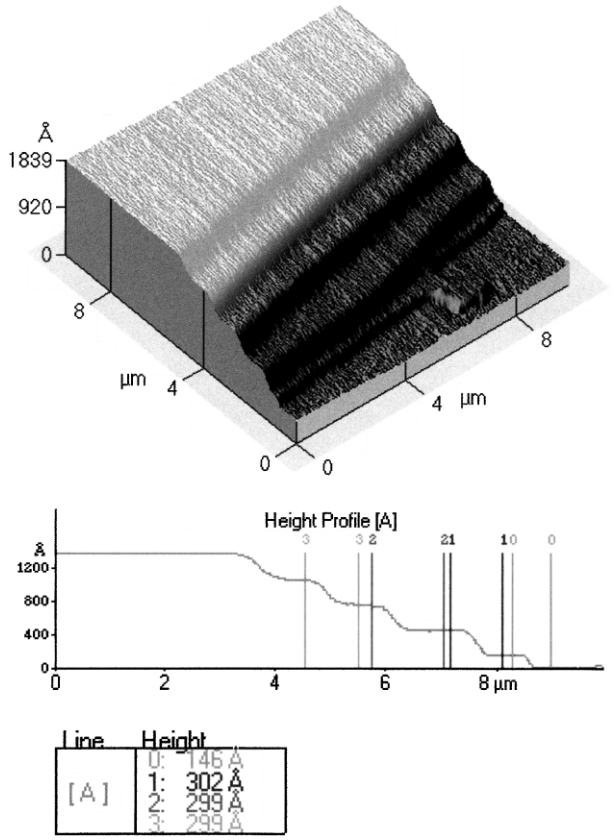

Fig. 7. Steps develop at the edge of a PS–b–PMMA film on SiO_x after it was annealed at 170°C for a few hours. The thickness of the step in contact with the substrate is 15 nm, whereas the other is 30 nm. The interlamellar spacing for this copolymer is $L_0 = 30$ nm.

ciently thick, then the features do not appear. We examined PS–b–PMMA ($N = 640$) samples in which the thickness gradually increased by a few hundred nanometers. We found that for this diblock copolymer films, the surface features do not exist above a thickness of 0.55 μm. This distance essentially is a measure of the effects of the surface interactions on the long-range orientation of the domains in the sample. Having completed a brief discussion of the ordering of thin film diblock copolymers, we are now in a position to discuss the behavior of thin film block copolymer/copolymer and block copolymer/homopolymer mixtures. All experiments described below concern copolymer/homopolymer thin film mixtures that are less that 2–3 L thick.

3.2. Copolymer / copolymer mixtures

We now consider a mixture of two symmetric diblock copolymers of different

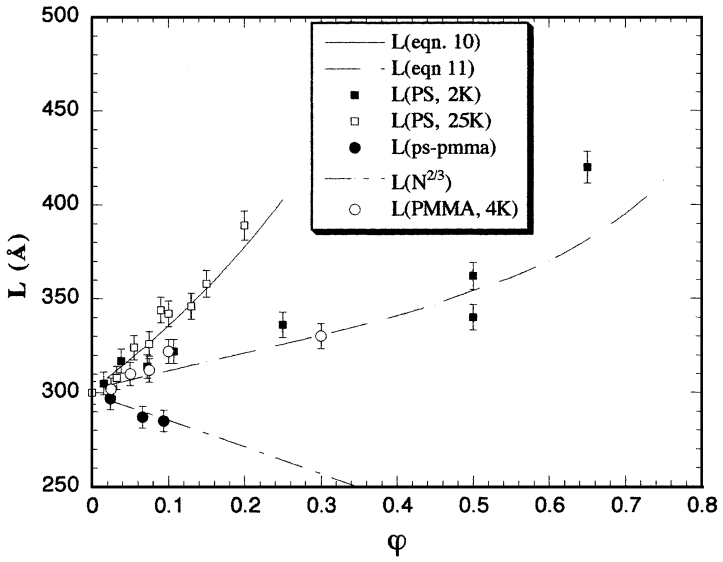

Fig. 8. The change in the interlamellar spacing of the $N = 640$ diblock copolymer with the addition of short–chain PS–b–PMMA diblock copolymers, with PS and with PMMA homopolymer chains is plotted here. φ is the volume fraction.

molecular weight, $N = 640$ and 200. Fig. 7 shows a scan of the edge of a PS–b–PMMA film on an SiO_x substrate. The height of the steps provides a measure of the interlamellar spacing. The average step height in this pure diblock ($N = 640$) is $L_o = 30$ nm, and the height of the layer in contact with the substrate, $L_1 = 15$ nm. The interlamellar spacing decreases with increasing weight fraction of the $N = 200$ molecular weight diblock copolymer, as shown in Fig. 8. Fundamentally, the lamellae shrink with increasing weight fraction of the lower molecular weight species because the short diblock segregates toward the PS/PMMA interfacial region in order to minimize unfavorable A/B contacts. In an effort to maintain a constant segmental density, the segments of the longer chain copolymer retract, thereby resulting in a decrease of the interlamellar spacing, as illustrated in Fig. 9. The line drawn through the data in Fig. 8 was computed by recognizing the relation between the weight fraction of the low molecular weight copolymer and the weight average molecular weight. This enables calculation of the dependence of L on φ, assuming that L is proportional to $N^{2/3}$ [Eq. (9)]. Using a dependence of $L \sim N^{1/2}$, that which is expected for a weakly segregated system [72,73], yields poor agreement.

The fact that L scales as $N^{2/3}$ instead of $N^{1/2}$ is of particular significance. Only in strongly segregated systems, $\chi N \gg 10.5$, is L proportional to $N^{2/3}$. One would assume that since the value of χN for the materials examined in this system is such that the materials are generally not considered strongly segregated, then the $N^{1/2}$ would be reasonable. However, the preferential interaction between the

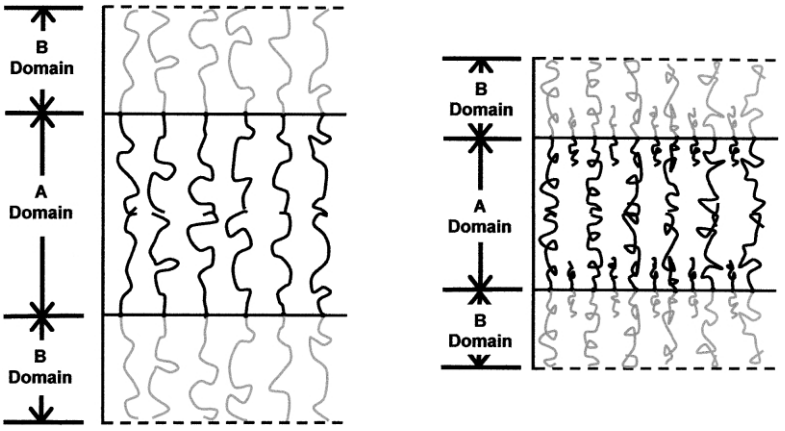

Fig. 9. The schematic illustrates how the domain size of an ordered diblock copolymer shrinks with the addition of chains that segregate toward the center of the domains.

PMMA component and the SiO_x substrate results in a higher degree of phase segregation of PMMA from the PS phase than in the bulk. In short, the interfacial region between the PS-rich and PMMA-rich phases is much narrower than a similar interface in the bulk. One might, alternatively, consider that the effective $\chi_{substrate}N$, near the substrate, is much larger than the bulk $\chi_{bulk}N$.

These results enable prediction of the interlamellar spacing for the $N = 200$ diblock copolymer, if it were ordered. For this copolymer, $L = 14$ nm, which is twice the brush height observed on SiO_x, as discussed in Section 3.1. It should be noted that despite the fact that the effective $\chi_{substrate}N$ may be large, the interlamellar spacing is not affected appreciably since L has a weak dependence on χ, $L \sim \chi^{/6}N^{2/3}$.

Finally, we should mention that we compared our data of interlamellar spacings with neutron reflectivity measurements of symmetric PS–b–PMMA diblock copolymer mixtures by Mayes et al. [71]. Our data are in excellent agreement (Fig. 10) with the neutron reflectivity data, indicating that the AFM technique provides a reliable analysis of the dimensions of phase separated domains by probing the topography of the sample.

3.3. Block copolymer / homopolymer mixtures

3.3.1. Background

We begin with a more detailed discussion of bulk mixtures of an A–b–B block copolymer with homopolymers A or B of different molecular weights [101–115]. This will allow us to later make a quantitative comparison of theory and experiment. The free energy is reduced when the homopolymers segregate to the appropriate domains of the ordered microstructure, reducing the number of unfavorable segmental A/B contacts. If the molecular weight of the homopolymer

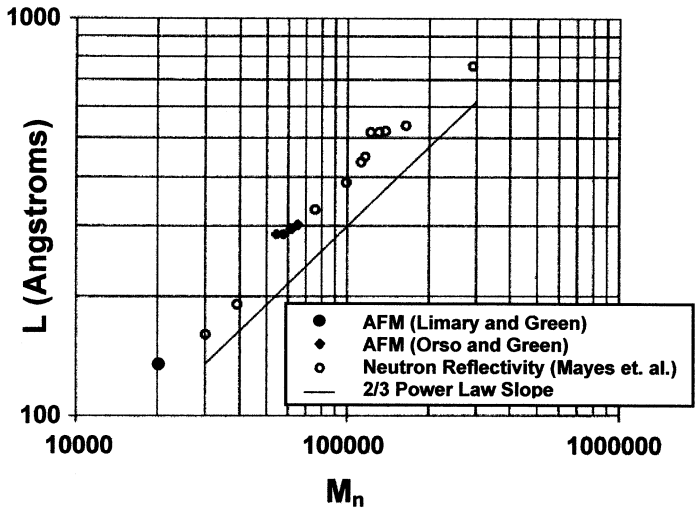

Fig. 10. These data show a comparison between the interlamellar spacings obtained from neutron reflectivity with those obtained using the AFM technique. The agreement is excellent. An extrapolation of the line to a molecular weight of 20, 500 ($N = 200$), indicates that the interlamellar spacing for a copolymer of this molecular weight, if it were ordered, would be approximately 14 nm.

is significantly less than that of the appropriate diblock component, the homopolymer chains interpenetrate the diblock 'brushes' and become distributed throughout the diblock domains. For these short homopolymer chains, the increase in translational entropy associated with mixing outweighs the slight decrease in conformational entropy resulting from the stretching of the copolymer chains to accommodate the homopolymer. If the homopolymer chains are uniformly distributed throughout the A-domain, the intermingling of the chains will cause the A-component of the diblock to stretch axially (perpendicular to the substrate) and also to swell laterally (parallel to the substrate). This lateral swelling increases the area per copolymer junction, which necessitates a shrinking of the B-domain in order to maintain uniform density throughout the film. The increase in the swelling of the A-domain offsets the shrinking of the B-domain and the net result is an increase in the interlamellar spacing. This is essentially the so-called 'wet brush' case discussed by Leibler [116]. A schematic is shown in Fig. 11a.

If the homopolymer is of comparable molecular weight to the diblock component, the homopolymer segregates to the middle of the corresponding diblock microdomain, resulting in a larger increase in the interlamellar spacing than the previous case. The diblock chains would have to stretch appreciably to allow the homopolymer chains to interpenetrate, resulting in a substantial decrease in the conformational entropy of the diblock chains. Increases in translational entropy of the homopolymer chains would not offset the increase in the elastic energy. Consequently, the copolymer 'brush' layers would not be interpenetrated by the homopolymer (the 'dry brush' condition) [116], see Fig. 11b. The other obvious

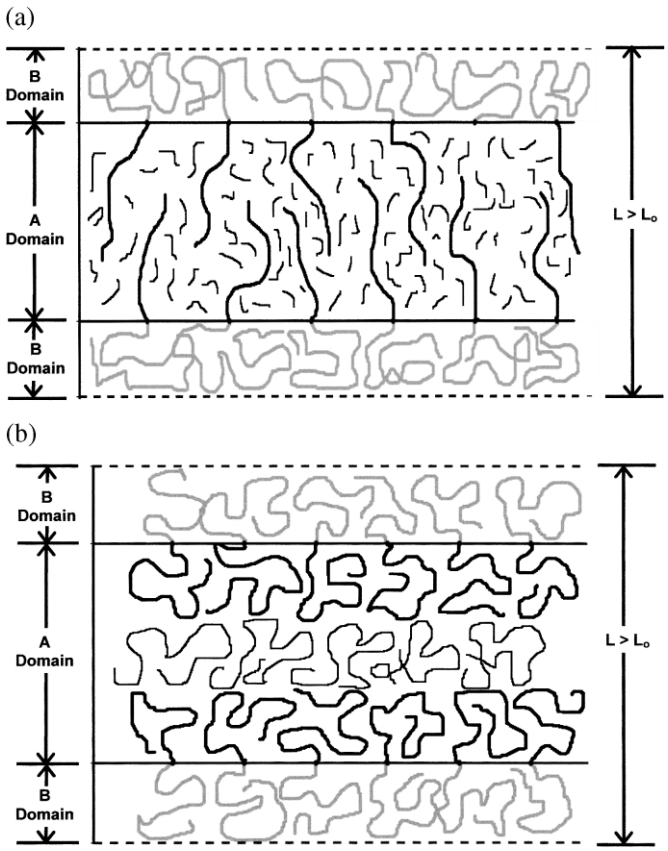

Fig. 11. Schematics of the PS–b–PMMA copolymer with (a) homopolymer chains distributed throughout one domain and (b) with homopolymer localized in the center of one domain.

situation arises when the homopolymer chains are long in comparison to the copolymer. Here it is well known that the homopolymer would form a separate phase.

Hamdoun et al. proposed a theoretical prediction for the behavior of nanosized inorganic particles incorporated into an ordered diblock copolymer [117]. The theory is, however, general, and not specific to the type of foreign component. The only requirement is that the copolymer and foreign component are non-interacting. If the added material is localized in the middle of the ordered microdomains, then the interlamellar spacing should increase with the volume fraction of homopolymer, φ, provided that the solubility limit is not exceeded:

$$L_{\text{localized}} = L_{\text{o}}/(1 - \varphi) \tag{10}$$

In this equation L_{o} is the interlamellar spacing of the pure diblock. On the other

hand, if homopolymer A is more uniformly distributed within the A-domain of the diblock, then Hamdoun et al. predict:

$$L_{\text{distributed}} = \frac{L_o[g(f,\varphi)]^{-1/3}}{(1-\varphi)} \tag{11}$$

where

$$g(f,\varphi) = \frac{f + (1-f)\varphi^2}{f(1-\varphi)^2}$$

In this equation, f is the volume fraction of the A-component in the diblock copolymer, which is $1/2$ for a symmetric diblock copolymer. Below we show how these predictions compare with theory.

3.3.2. Copolymer (A–b–B) / homopolymer A or B mixtures

The effect of surface constraints on the phase behavior of thin film PS/PS–b–PMMA and PMMA/PS–b–PMMA mixtures in relation to the behavior of the relevant bulk systems is now discussed. Recall that in this system, the PS component has a lower surface energy and segregates to the free surface whereas the PMMA component resides at the SiO_x substrate. PS and PMMA homopolymers, as well as a 5-norbornene-2-methyl-d_3-carboxylate (NBMC) homopolymer of degree of polymerization of $N_{\text{NBMC}} \approx 174$ with $M_w/M_n < 1.025$, were mixed with the PS–b–PMMA diblock copolymer of degree of polymerization $N = 640$. The NBMC was synthesized by living ring-opening metathesis polymerization (ROMP) of 5-norbornene-2-methyl-d_3-carboxylate [69]. Different molecular weight PS and PMMA homopolymers were used in order to examine the role of the entropic contribution to the phase behavior. The substrates included: silicon, with a native oxide layer approximately 2 nm thick; titanium nitride; and an iron tellerium oxide glass, synthesized in our laboratory.

We first consider the PS($N = 250$)/PS–b–PMMA mixture. Fig. 8 shows that the interlamellar spacing increases with the volume fraction of PS ($N = 250$). Eq. (10), which assumes that the homopolymer is segregated toward the middle of the PS domain, describes the data well. This agreement is expected since the homopolymer chain length is comparable to the PS chain length in the copolymer (Fig. 11a). Entropy restricts the interpenetration of the copolymer brush layers by the large homopolymer chains.

L increases more slowly with increasing φ for the PS ($N = 20$)/PS–b–PMMA than the PS($N = 250$)/PS–b–PMMA samples. This is to be expected if the low molecular weight chains are more evenly distributed throughout the PS domains (Fig. 11a). The line drawn through the open squares in Fig. 8 was computed using Eq. (11), which assumes such to be the case. It is noteworthy that the topographies of the samples remained identical for PS volume fractions of up to 65%, indicating that the lamellar structure was maintained. A bulk mixture of the same system

would be expected to have undergone an order–order (lamellar to cylindrical) transition as the overall composition deviated substantially from the 50:50 [103–106]. This is not the case in these thin films of $h < 2L$, where the structure remains lamellar.

At higher volume fractions, beyond 65%, however, the topographical features disappear. In fact, the excess PS homopolymer chains segregate toward the free surface and the PS–b–PMMA segregated preferentially to the polymer/substrate interface, as expected [118,119]. These results indicate that the polymer/substrate interactions are sufficiently strong in order to maintain the lamellar morphology. Evidently, order–order transitions can be frustrated in thin films in relation to the bulk, depending on the nature of the polymer segmental interactions with the substrate. When the solubility limit is reached, the homopolymer chains segregate to the free surface. The effects of the substrate will diminish rapidly with increasing film thickness.

We now comment on the structural stability of the system. Thin PS films are inherently unstable on the SiO_x substrate and will dewet spontaneously to create droplets. However, the thin film is stable when blended with PS–b–PMMA diblock copolymer, as the minor component of the film. The stability occurs because the diblock copolymers preferentially segregate to the substrate, creating a layer than acts as an 'anchor' [119].

Additional constraints on the lamellar layer in contact with the substrate, relative to other layers in the sample, also affect the domain dimensions. In the case of the PS($N = 250$) sample, the height of the first step decreased slightly from $L_1 = L_0/2$ with increasing PS($N = 250$) contents whereas it increased to 17.5 nm at sufficiently large PS($N = 20$) homopolymer contents. This is consistent with the fact that the PS($N = 250$) homopolymer chains do not penetrate the brush in the first layer. The slight decrease in L_1 with increasing PS($N = 250$) is evidently the result of the constraint on the system to maintain a constant segmental density. However, in the case of the PS($N = 20$), the short chain homopolymer is able to penetrate the 'brush', thereby swelling it. Fig. 12 illustrates the situation for short chain homopolymers.

3.3.3. Effect of substrate / polymer interaction on miscibility

We now examine the influence of substrate/polymer interaction on miscibility. The height of the first layer, L_1, when the PS–b–PMMA ($N = 640$) diblock copolymer was in contact with titanium nitride or with iron–tellerium glass was 30 nm. All other layers are of height 30 nm. This indicates that the PS component resides at the free surface and at the substrate. The thickness of the other layers increased with increasing PS(25K) homopolymer content in a manner consistent with the results described above when SiO_x was the substrate, as expected. However, at low concentrations, L_1 exhibited a larger rate of increase with φ for films on TiN or on tellerium substrates, than on SiO_x substrates. This increase in L_1 was not due to interpenetration of homopolymer into the PS brush in the first layer, since interpenetration would be prohibited based on entropic considerations. The increase is reconciled by the fact that the PS homopolymer have the translatio-

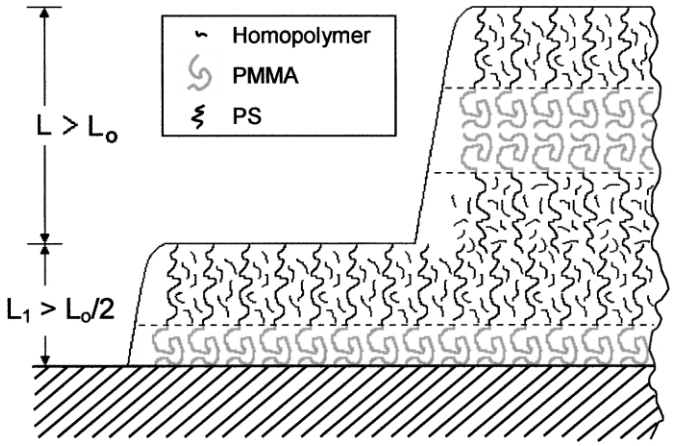

Fig. 12. This schematic shows the interpenetration of the copolymer layers in the vicinity of the substrate by short homopolymer chains.

nal freedom to segregate to the polymer/substrate interface, thereby showing an artificial increase in L_1.

While the behavior of the PMMA(4K)/PS–b–PMMA mixture was similar to that of the PS(2K)/PS–b–PMMA mixture in that Eq. (11) provided an excellent description of the dependence of L on φ in both cases, there is one important distinction. For low mwt. PMMA/copolymer thin film mixtures, the first layer (in contact with SiO_x) rapidly increased to 18 nm whereas it remains constant in the low mwt. PS homopolymer/copolymer mixtures. The increase in L_1 is the result of the translational freedom of the PMMA homopolymer chains to segregate to the SiO_x substrate. We note that a similar observation was made for in the SiO_x/PS–b–PMMA/NBMC mixture, as discussed in the section that follows.

3.3.4. Block copolymer (A–b–B) / homopolymer C mixtures

The addition of NBMC homopolymer increased the interlamellar spacing in the PS–b–PMMA mixture, though not nearly to the degree of the PS homopolymer, Fig. 13. These data show that at small φ, the increase is well described by the solid line computed using Eq. (11), indicating that the homopolymer chains are preferentially located in one domain and do not interpenetrate the brush layers. When $\varphi > 0.05$, L becomes independent of φ. The broken line in Fig. 13 reflects a constant value for L and serves to emphasize the fact that L is constant for $\varphi > 0.05$. We observe from the figure that L_1 increases significantly in this system for $\varphi > 0.05$.

The reason for this large increase in L_1 is now described. NBMC is incompatible with PS, and with PMMA, in binary NBMC/PS and NBMC/PMMA mixtures. It has a stronger affinity for the silicon substrate than either PS or PMMA. Ion beam analysis measurements of binary mixtures of PS/NBMC and PMMA/NBMC show

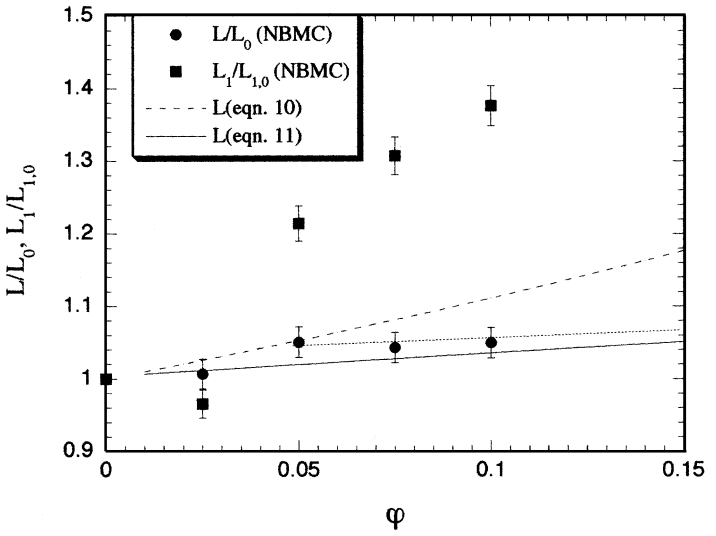

Fig. 13. The dependence of the interlamellar spacing, L, with the addition of NBMC homopolymer volume fraction, φ, is shown here. The thickness, L_1, of the layer in contact with the substrate, increases at a faster rate with φ than do other layers L.

that the NBMC segregates to the silicon substrate, and PS or PMMA would segregate to the free surface [69]. Therefore it would appear that for very small homopolymer concentrations, the NBMC chains are predominantly localized at the center of the PMMA ordered domains. However, once the solubility limit has been exceeded, $\varphi > 0.05$, NBMC chains rapidly form a separate phase at the substrate/copolymer interface. Independent secondary ion mass spectrometry measurements confirm the preferential segregation of the NBMC component to the substrate [69]. Essentially the diblock copolymer forms an ordered structure on a thin layer of NBMC. Considering that the thickness of the layer in contact with the NBMC layer is comparable to $L_0/2$ and not L_0, and that the layer at the free surface has to be PS, then it is reasonable to conclude that PMMA is in contact with the NBMC layer. These data suggest that the PMMA component is slightly more compatible with the NBMC than PS under these conditions.

We now consider the influence of the substrate by investigating the behavior of the mixture on the iron tellurium glass and on TiN. The PS component resides at the copolymer/TiN and at copolymer/tellurium interfaces because $L_1 = L$. Independent ion beam analysis measurements reveal that PS has a preferential affinity for the free surface over NBMC [69]. Therefore, the NBMC homopolymer must reside within the thin film diblock structure. AFM measurements indicate that the block copolymer domains shrink rather than swell! The shrinking is reconciled by the fact that the chains are forced to distribute themselves preferentially throughout the PS/PMMA interfacial regions of the sample. This is in contrast to the

situation involving the SiO_x substrate for which PMMA had a preferential attraction. Clearly, the substrate interactions influence miscibility in these systems.

4. Conclusions

Two topics in the area of block copolymer thin films were discussed:

1. Pattern formation in a thin diblock copolymer film in a temperature range above the order–disorder transition temperature
2. Phase behavior of ordered thin film symmetric diblock copolymer/homopolymer mixtures.

A symmetric diblock copolymer in the temperature range $T > T_{ODT}$ exhibits interfacial properties that are akin to those of simple homopolymer thin films, yet retains properties that are inherently associated with block copolymers. PS–b–PMMA diblock copolymers of $\chi N < 10.5$ underwent a surface-induced ordering on SiO_x substrate. Polar interactions of the PMMA component with SiO_x results in the formation of a brush of height h_L, one-half the interlamellar spacing, $L_0/2$, of the diblock in its ordered state. Films with $h < 7$ nm ($L_0/2$), underwent a structural instabilities, whereby they dewet the SiO_x substrate via a conventional nucleation and growth process or by the formation of a bicontinuous structure, depending on actual value of h. Films with 7 nm $< h <$ 35 nm exhibit an 'autophobic' dewetting process whereby a layer of thickness $h_d = h - h_L$ dewets an underlying layer of thickness 7 nm. The pattern comprises a 'bicontinuous' structure when 7 nm $< h <$ 19 nm, or holes if 19 nm $< h <$ 35 nm. In short, a hierarchy of transient structures are created at the surface of the film when the film thickness is $T > T_{ODT}$. These structures are believed to be the result of long-range intermolecular forces.

Topographical features are spontaneously created in ordered copolymer films ($\chi N > 10.5$ or $T < T_{ODT}$). However, the topographical features remain at a constant height, L, reflective of the inherent length scale (interlamellar spacing) associated with phase separation in the system. The thermodynamic interactions have a stabilizing effect on the structure of the film when $\chi N > 10.5$, hence the structure does not evolve to form droplets, as is the case for the block at $T > T_{ODT}$. It should be cautioned however that if the A/B, segment/segment, interactions in the diblock are more favorable than A/substrate or B/substrate interactions, then ultra thin films of copolymers in the range $\chi N > 10.5$ could dewet. This follows from the fact that near the surface, the energy is minimized when more A/B segment/segment contacts are created in order to reduce the number of polymer segment/substrate interactions. Thicker films would, of course, be stable because any destabilizing effects of long-range interactions should diminish.

Since the dimensions of the topographical features provide a measure of the inherent length scales describing the phase separated structure, they enable

determination of the change in domain dimensions with homopolymer concentration in symmetric copolymer/homopolymer systems. This proved to be an effective means to examine the influence of polymer/substrate interactions on miscibility in thin film blends. To this end, we examined thin film mixtures of a PS–b–PMMA diblock copolymer with PS and PMMA homopolymers of different molecular weights and with NBMC homopolymer. The NBMC homopolymer is incompatible with PS and with PMMA homopolymers in binary, PS/NBMC and PMMA/NBMC, mixtures. In these NBMC/copolymer mixtures, miscibility is influenced by the relative polymer segment/segment and segment/substrate interactions. Order–order transitions appear be frustrated in these thin film mixtures due to the influence of the polymer segment/substrate interactions. Finally, we showed that the dependence of the microphase-separated domain size on the homopolymer volume fraction depends on the proximity of the layer from the substrate.

Acknowledgements

This work was supported by the National Science Foundation (DMR-0072898) and by the Robert A. Welch Foundation.

References

[1] J.J. Halls, C.A. Walsh, N.C. Greenham et al., Nature 376 (1995) 498.
[2] V.N. Bliznyuk, S.A. Carter, J.C. Scott, G. Klarner, R.D. Miler, D.C. Miller, Macromolecules 32 (1999) 369.
[3] J.L. Keddie, R.A.L. Jones, R.A. Cory, Faraday Discuss. 98 (1994) 219.
[4] J.A. Forrest, K. Dalnoki-Veress, J.R. Dutcher, Phys. Rev. E 58 (1998) 6119.
[5] J.A. Forrest, K. Dalnoki-Vress, J.A. Dutcher, Phys. Rev. E 56 (1997) 5706.
[6] J.A. Forrest, C. Svanberg, K. Revesz, M. Rodahl, L.M. Torrell, B. Kasemo, Phys. Rev. E 58 (1998) R1226.
[7] W.E. Wallace, J.H. van Zanten, W.L. Wu, Phys. Rev. E 52 (1995) R3329.
[8] J.L. Keddie, R.A.L. Jones, R.A. Cory, Europhys. Lett. 27 (1) (1994) 59.
[9] J.A. Forrest, K. Dalnoki-Veress, J.R. Stevens, J.R. Dutcher, Phys. Rev. Lett. 77 (2002) 1996.
[10] A.L. Demirel, S. Granick, Phys. Rev. Lett. 77 (1996) 2261.
[11] G. Luengo, F.-J. Schmitt, R. Hill, J. Israelachvili, Macromolecules 30 (1997) 2482.
[12] Y. Lu, T.P. Russell, M.G. Samant et al., Macromolecules 30 (1997) 7766.
[13] B. Frank, A.P. Gast, T.P. Russell, H.R. Brown, C. Hawker, Macromolecules 29 (1996) 6531.
[14] H.R. Brown, T.P. Russell, Macromolecules 29 (1996) 798.
[15] D.B. Hall, J.M. Torkelson, Macromolecules 31 (1998) 8817.
[16] J.G. Van Alsten, B.B. Sauer, D.J. Walsh, Macromolecules 25 (1992) 4046.
[17] X. Zheng, M.H. Rafailovich, J. Sokolov et al., Phys. Rev. Lett. 79 (1997) 241.
[18] K. Binder, Adv. Polym. Sci. 138 (1999) 1.
[19] A. Werner, M. Muller, F. Schmid, K. Binder, J. Chem. Phys. 110 (2) (1999) 1221.
[20] T. Kearle, J. Klein, K. Binder, Phys. Rev. Lett. 77 (1996) 1318.
[21] A. Werner, F. Schmid, M. Muller, K. Binder, J. Chem. Phys. 107 (19) (1997) 8175.
[22] S. Puri, K. Binder, H.L. Frisch, Phys. Rev. E 56 (1997) 6991.
[23] M. Sferraza, C. Xiao, R.A.L. Jones, Phys. Rev. Lett. 78 (1997) 3693.
[24] J. Genzer, R.J. Composto, J. Chem. Phys. 106 (3) (1997) 1257.
[25] I. Schmidt, K. Binder, J. Physique 46 (1985) 1631.

[26] M. Sikka, N. Singh, A. Karim, F.S. Bates, S.K. Satija, C.F. Majkrzak, Phys. Rev. Lett. 70 (1993) 307.
[27] H. Tanaka, Europhys. Lett. 24 (8) (1993) 665.
[28] J. Heier, E.J. Kramer, P. Revesz, G. Battisig, F.S. Bates, Macromolecules 32 (1999) 3758.
[29] M. Okada, H. Oshima, T. Chiba, T. Nose, Macromolecules 28 (1995) 4759.
[30] A. Saout-Elhak, M. Benhamou, M. Daoud, J. Phys. II Fr. 7 (1997) 503.
[31] K. Tanaka, J.-S. Yoon, A. Takahara, T. Kajiama, Macromolecules 35 (1995) 934.
[32] B.D. Ermi, A. Karim, J.F. Douglas, J. Polym. Sci. Part B Polym. Phys. 36 (1998) 191.
[33] W. Guo, J.S. Higgins, Polymer 31 (1990) 699.
[34] A. Budkowski, U. Steiner, J. Klein, J. Chem. Phys. 97 (7) (1992) 5229.
[35] S. Reich, Y. Cohen, J. Polym. Sci. Polym. Phys. Ed. 19 (1981) 1255.
[36] Y. Rouault, J. Kaschnagel, K. Binder, J. Stat. Phys. 80 (1995) 1009.
[37] U. Steiner, G. Krausch, G. Schatz, J. Klein, Phys. Rev. Lett. 64 (1990) 119.
[38] H. Tang, I. Szleifer, S.K. Kumar, J. Chem. Phys. 100 (7) (1994) 5367.
[39] G. Brown, A. Chakrabarti, Phys. Rev. A 46 (1992) 4829.
[40] F. Bruder, R. Brenn, Phys. Rev. Lett. 69 (1992) 624.
[41] L. Sung, A. Karim, J.F. Douglas, C.C. Han, Phys. Rev. Lett. 76 (1996) 4369.
[42] G. Krausch, E.J. Kramer, F.S. Bates, J.F. Marco, G. Brown, A. Chakabarti, Macromolecules 27 (1994) 6768.
[43] G. Krausch, C.-A. Dai, E.J. Kramer, J.F. Marko, F.S. Bates, Macromolecules 26 (1993) 5566.
[44] D. Slep, J. Asselta, M.H. Rafailovich et al., Langmuir 14 (1998) 4860.
[45] K.D. Jandt, J. Heir, F.S. Bates, E.J. Kramer, Langmuir 12 (1996) 3716.
[46] A. Karim, J.F. Douglas, B.P. Lee et al., Phys. Rev. E 57 (1998) R6273.
[47] G. Nisato, B.D. Ermi, J.F. Douglas, A. Karim, Macromolecules 32 (1999) 2356.
[48] A. Karim, T.M. Slawecki, S.K. Kumar et al., Macromolecules 31 (1998) 857.
[49] M. Boltau, S. Walheim, J. Mylnek, G. Krausch, U. Steiner, Nature 391 (1998) 877.
[50] E. Huang, T.P. Russell, C. Harrison et al., Macromolecules 31 (1998) 7641.
[51] E. Huang, S. Pruzinsky, T.P. Russell, J. Mays, C.J. Hawker, Macromolecules 32 (1999) 5239.
[52] P. Bassereau, D. Brodrick, T.P. Russell, H.R. Brown, K. Shull, Phys. Rev. Lett. 71 (1993) 1716.
[53] P. Mansky, J. DeRouchey, T.P. Russell et al., Macromolecules 31 (1998) 4399.
[54] A. Halperin, J.U. Sommer, M. Daoud, Europhys. Lett. 29 (1995) 297.
[55] T.L. Morkved, H.M. Jaeger, Europhys. Lett. 40 (1997) 643.
[56] P.F. Green, T.M. Christensen, T.P. Russell, Macromolecules 24 (1991) 252.
[57] B. Collin, D. Chatenay, G. Coulon, D. Ausserre, Y. Galott, Macromolecules 25 (1992) 1621.
[58] P. Lambooy, T.P. Russell, G.J. Kellog, A.M. Mayes, P.D. Gallagher, S.K. Satija, Phys. Rev. Lett. 72 (1994) 2899.
[59] G.J. Kellog, D.G. Walton, A.M. Mayes, et al., Phys. Rev. Lett. 76 (1996) 2503.
[60] A. Menelle, T.P. Russell, S.H. Anastasiadis, S.K. Satija, C.F. Majkrzak, Phys. Rev. Lett. 68 (1992) 67.
[61] M.A. van Dijk, R. van den Berg, Macromolecules 28 (1995) 6773.
[62] N. Gadegaard, K. Almadal, N.B. Larsen, K. Mortensen, Appl. Surf. Sci. 142 (1999) 608.
[63] A. Karim, N. Singh, M. Sikka, F.S. Bates, J. Chem. Phys. 100 (2) (1994) 1620.
[64] N. Koneripalli, R. Levicky, F.S. Bates, J. Anker, H. Kaiser, S.K. Satija, Langmuir 12 (1996) 6681.
[65] P. Mansky, T.P. Russell, C.J. Hawker, J. Mays, D.C. Cook, S.K. Satija, Phys. Rev. Lett. 79 (1997) 237.
[66] S.T. Milner, D.C. Morse, Phys. Rev. E 54 (1996) 3793.
[67] M.W. Matsen, J. Chem. Phys. 106 (18) (1997) 7781.
[68] M.W. Matsen, Phys. Rev. Lett. 74 (1995) 4225.
[69] M.D. Smith, R.A. Saunders, P.F. Green, Macromolecules 32 (1999) 8392.
[70] K.A. Orso, P.F. Green, Macromolecules 32 (1999) 1087.
[71] A.M. Mayes, T.P. Russell, V.R. Deline, S.K. Satija, C.F. Majkrzak, Macromolecules 27 (1994) 7447.
[72] I.W. Hamley, The Physics of Block Copolymers, Oxford Univ. Press, New York, 1998.
[73] F.S. Bates, G.H. Fredrickson, Annu. Rev. Phys. Chem. 41 (1990) 525.

[74] F. Brochard-Wyart, P. Martin, C. Redon, Langmuir 9 (1993) 3682.
[75] G. Reiter, A. Sharma, R. Khanna, A. Casoli, M.-O. David, J. Colloid Intf. Sci. 214 (1999) 126.
[76] R.A. Segalman, P.F. Green, Macromolecules 32 (1999) 801.
[77] F. Brochard-Wyart, J. Daillant, Can. J. Phys. 68 (1990) 1084.
[78] R. Xie, A. Karim, J.F. Douglas, C.C. Han, R.A. Weiss, Phys. Rev. Lett. 81 (1998) 1251.
[79] A. Sharma, R. Khanna, J. Chem. Phys. 110 (10) (1999) 4929.
[80] J.-L. Masson, P.F. Green, J. Chem. Phys. 112 (2000) 349.
[81] A. Michev, K. Binder, J. Chem. Phys. 106 (1997) 1978.
[82] R. Limary, P.F. Green, Macromolecules 32 (1999) 8167.
[83] T.P. Witelski, A.J. Bernoff, Phys. Fluids 11 (1999) 2443.
[84] R.M. Overney, D.P. Leta, L.J. Fetters, J. Vac. Sci. Technol. B 14 (2) (1996) 1276.
[85] R. Yerushalmi-Rosen, J. Klein, L.J. Fetters, Science 263 (1994) 793.
[86] C. Yuan, M. Ouyang, J.T. Koberstein, Macromolecules 32 (1999) 2329.
[87] F. Brochard-Wyart, G. Debregeas, R. Fondecave, P. Martin, Macromolecules. 30 (1997) 1211.
[88] M. Sferrazza, M. Heppenstall, R. Cubitt, D. Bucknall, J. Webster, R.A.L. Jones, Phys. Rev. Lett. 81 (1998) 5173.
[89] G. Reiter, A. Sharma, A. Casoli, M.-O. Davis, R. Kahanna, P. Auroy, Langmuir 15 (1999) 1551.
[90] I.W. Hamley, E.L. Hiscutt, Y.-W. Yang, C. Booth, J. Colloid Intf. Sci. 209 (1999) 255.
[91] S. Qu, C.J. Clarke, Y. Lin et al., Macromolecules 30 (1997) 3640.
[92] G. Reiter, P. Auroy, L. Auvray, Macromolecules 29 (1996) 2150.
[93] P. Martin, A. Buguin, F. Brochard-Wyart, Eur. Phys. Lett. 28 (1994) 421.
[94] F. Brochard-Wyart, P. Martin, C. Redon, Langmuir 9 (1993) 3682.
[95] G. Reiter, Phys. Rev. Lett. 68 (1992) 75.
[96] R. Limary, P.F. Green, Langmuir 15 (1999) 5617.
[97] T. Kearle, R. Yerushalmi-Rosen, J. Klein, Europhys. Lett. 38 (1997) 207.
[98] M. Schneemilch, R.A. Hayes, J.G. Petrov, J. Ralston, Langmuir 14 (1998) 7047.
[99] E. Tomasetti, P.G. Rouxhet, R. Legras, Langmuir 14 (1998) 3435.
[100] M.D. Whitmore, J. Noolandi, Macromolecules 18 (1985) 2486.
[101] M. Banaszak, M.D. Whitmore, Macromolecules 25 (1992) 2757.
[102] K.M. Hong, J. Noolandi, Macromolecules 16 (1983) 1083.
[103] K.I. Winey, E.L. Thomas, L.J. Fetters, Macromolecules 24 (1991) 6182.
[104] K.I. Winey, E.L. Thomas, L.J. Fetters, Macromolecules 25 (1992) 2645.
[105] K.I. Winey, E.L. Thomas, L.J. Fetters, J. Chem. Phys. 95 (1991) 9367.
[106] W.C. Zin, R.J. Roe, Macromolecules 17 (1984) 183.
[107] R.J. Roe, W.C. Zin, Macromolecules 17 (1984) 189.
[108] M.W. Matsen, Macromolecules 28 (1995) 5765.
[109] H. Tanaka, H. Hasegawa, T. Hashimoto, Macromolecules 24 (1991) 240.
[110] T. Hashimoto, H. Tanaka, H. Hasegawa, Macromolecules 23 (1990) 4378.
[111] P.S. Tucker, J.W. Barlow, D.R. Paul, Macromolecules 21 (1988) 2794.
[112] P.S. Tucker, D.R. Paul, Macromolecules 21 (1988) 2801.
[113] Y. Feng, A. Karim, R.A. Weiss, J.F. Douglas, C.C. Han, Macromolecules 31 (1998) 484.
[114] K.I. Winey, E.L. Thomas, L.J. Fetters, Macromolecules 25 (1992) 422.
[115] A.-C. Shi, J. Noolandi, Macromolecule 27 (1994) 2936.
[116] L. Leibler, Macromol. Chem. Macromol. Symp. 16 (1988) 1.
[117] B. Hamdon, D. Aussere, V. Cabuil, S. Joly, J. Phys. II 6 (1996) 503.
[118] P.F. Green, T.P. Russell, Macromolecules 24 (1991) 2931.
[119] P.F. Green, T.R. Russell, Macromolecules 25 (1992) 783.